Low-Cycle Fatigue Behavior of NIMONIC PE16 at Room Temperature

V. SINGH, M. SUNDARARAMAN, W. CHEN, and R.P. WAHI

The fatigue behavior of NIMONIC PE16 has been investigated at room temperature as a function of γ' particle size (from 10 to 30 nm) and total strain amplitude (0.44 to 2.60 pct). All specimens initially harden and then soften on further deformation. The degrees of hardening and softening show a marked variation with γ' particle size and strain amplitude. Cyclic stress-strain and Coffin-Manson plots show a bilinear behavior with a change of slope at $\Delta\varepsilon_p/2$, the plastic strain amplitude, of about 0.3 pct. These results are interpreted in terms of microstructural observations, namely, the number of slip systems activated and mutual interaction of dislocations on these systems, as well as their interaction with γ' particles.

I. INTRODUCTION

THE low-cycle fatigue (LCF) behavior of pure metals and alloys has been extensively studied.[1,2] Detailed investigations have also been made on the fatigue behavior of some simple age-hardenable systems, like CuCo strengthened by Co precipitates[3] and Al-Cu strengthened by θ'' precipitates.[4,5] Extensive studies have also been made on the fatigue behavior of nickel-base alloys containing large volume fractions of the strengthening phase γ'.[6-9] The γ' phase has a $L1_2$ structure and a nominal composition of $Ni_3(Al, Ti)$. However, relatively few investigations have been carried out on nickel-base alloys containing small volume fractions of γ'.[10-15] Most of the researchers have confined their study to fatigue behavior either as a function of some particular parameters of testing or particle size.[11-15] Lerch *et al.*[10] have studied the influence of γ' particle size and grain size on the fatigue damage mechanisms in WASPALOY* as tested between 300 and 1073 K.

In the present investigation, a nickel-base superalloy, NIMONIC** PE16, has been chosen because of its relatively simple microstructure consisting of a uniform distribution and a low volume fraction (maximum about 12 pct) of γ' particles.[16] The high-temperature LCF behavior of this alloy has recently been reported by Wahi *et al.*[17] The room-temperature LCF behavior, particularly the cyclic stress response, stress-strain relationship, and fatigue life, is critically examined as a function of γ' particle size [underaged (UA) to overaged (OA) state] and also of total strain amplitude. The results are discussed in the light of microstructural observations. The cyclic stress-strain relationship has been briefly reported earlier.[18]

*WASPALOY is a trademark of Precision Rings, Inc., Indianapolis, IN.

**NIMONIC is a trademark of Inco Alloys International, Inc., Huntington, WV.

V. SINGH, Professor, is with the Department of Metallurgical Engineering, Institute of Technology, Banaras Hindu University, Varanasi 221 005, India. M. SUNDARARAMAN, Scientist, is with the Physical Metallurgical Division, Bhabha Atomic Research Center, Bombay 85, India. W. CHEN, Scientist, is with the Institut für Metallforschung, Technische Universität Berlin, 1000 Berlin 12, Federal Republic of Germany. R.P. WAHI, Professor, is with the Hahn-Meitner-Institut Berlin, 1000 Berlin 39, Federal Republic of Germany.

Manuscript submitted July 5, 1989.

II. EXPERIMENTAL

The alloy, NIMONIC PE16, used in the present investigation was supplied by M/S Glossop Superalloys Ltd., Glossop Derbyshire, United Kingdom. The chemical composition of the alloy is given is Table I. Blanks of 98-mm length and 22.4-mm diameter were solutionized at 1313 K for 1/2 hour to produce uniform, equiaxed grains of about 30 μm and subsequently aged at 1023 K for different periods of time to produce γ' particles of various sizes. Measurements of diameter and number density of the γ' precipitates were made on transmission electron microscopy (TEM) micrographs. To derive the average diameters and the volume fractions of the γ' precipitates, the measured values were corrected for the errors introduced due to the geometry of the TEM specimens.[16] All of the heat-treatment procedures applied produce a constant volume fraction of 7 pct.[16] Details of heat treatment and resulting γ' sizes are listed in Table II. The state of aging (UA, underaged; PA, peak aged; and OA, overaged) referred to in Table II is based on an earlier work.[16]

Button head-type LCF specimens having a gage length of 13 mm, a gage diameter of 8 mm, and shoulder radii of 7 mm were machined from the heat-treated blanks. The gage section was mechanically polished longitudinally to a surface finish of $Ra = 2.5 \pm 0.5$ μm. Fatigue tests were conducted in an axial strain control mode under fully reversed push-pull loading ($R = -1$) in a servo-hydraulic machine. Different total strain amplitudes from 0.44 to 2.60 pct (plastic strain amplitudes from 0.14 to 2.1 pct) and a constant nominal strain rate of 4×10^{-3}/s were employed. All of the tests were carried out in air at room temperature. A triangular waveform was used, and all of the tests were begun in tension. The strain was monitored by a 12-mm clip-on, high-temperature extensometer mounted in the gage section. The load response was continually measured. The number of cycles to cause complete failure is taken as fatigue life, N_f.

All of the specimens were examined by optical and electron microscopy to study the fatigue-induced deformation microstructure. Samples for optical microscopy

Table I. Chemical Composition (Weight Percent) of NIMONIC Alloy PE16

C	Si	Mn	Ni	Co	Cr	Mo	Ti	Al	Zr	B	S (ppm)	Fe
0.05	<0.05	<0.05	42.6	<0.05	16.3	3.4	1.35	1.27	<0.02	0.003	5	bal.

were prepared by mechanical polishing and subsequent etching in a solution containing five parts of HCl and one part HNO_3. Specimens for electron microscopy were prepared with the foil surface normal to the tensile axis. Standard specimen preparation technique was employed.[16]

III. RESULTS

A. *Initial Microstructure*

A homogeneous distribution of spherical coherent γ' particles in the face-centered cubic (fcc) matrix was observed in the heat-treated condition (Figure 1). Grain boundaries were found to be decorated with $M_{23}C_6$-type carbides identified with the help of selected area diffraction (SAD). The aging time employed in the present study did not produce any significant change in the average size and size distribution of the carbides. Carbides of the types M(C, N) and M_6C were also observed. Total volume fraction of the carbides amounted to about 1 pct.[16]

B. *LCF Behavior*

Stress response curves ($\Delta\sigma/2$ *vs* number of cycles at a fixed total strain amplitude) displayed increasing hardening during initial cycles to a maximum value, followed by a gradual stress drop with further deformation. This characteristic behavior was exhibited at all strain amplitudes and γ' particle sizes. All relevant test results are shown in Table III. A typical stress response curve for PA material (21-nm γ' particle size) for different total strain amplitudes $\Delta\varepsilon_t/2$ is plotted in Figure 2. The maximum stress for small strain amplitudes ($\Delta\varepsilon_t/2 \leq 0.70$ pct) is attained within a narrow range (by about 30 cycles), whereas at large strain amplitudes ($\Delta\varepsilon_t/2 > 0.70$ pct), the number of cycles required to achieve a stress maximum shifts rapidly to lower cycle values. Underaged material also exhibits a similar behavior. However, in the case of OA material (30-nm γ' particle size), the stress maximum continually shifts to a smaller number of cycles with increasing strain amplitude (Table III).

In the present study, tests have been carried out in a total strain control mode. The plastic strain amplitude varies during the test, showing a minimum value at the maximum stress. Therefore, to understand the cyclic stress response, the stress amplitude $\Delta\sigma/2$ is plotted in Figure 3 against cumulative plastic strain $\Sigma\Delta\varepsilon_p(\approx 2 \cdot \Delta\varepsilon_p \cdot N)$ for all of the γ' sizes and two values of $\Delta\varepsilon_t/2$. These plots are typical examples of stress response curves for the small and large strain amplitude regimes, respectively. For small strain amplitudes, the maximum stress increases with increasing γ' particle size up to PA condition and decreases thereafter (OA state). The cumulative plastic strain at which the maximum stress is achieved increases with increasing particle size. Stress response curves for specimens tested at large strain amplitudes (*e.g.*, $\Delta\varepsilon_t/2 \approx 2.60$ pct) reveal many interesting features: (1) Unlike at small strain amplitudes, the stress maximum is achieved at comparable cumulative plastic strain for all γ' particle sizes, and the stress response curves of UA and PA merge together; (2) the value of the maximum stress is smaller for the OA material; and (3) at higher cumulative plastic strain, the stress response curve of OA material also merges with those of UA and PA materials. For all strain amplitudes, the degree of hardening, defined as the difference between the maximum stress and the 0.2 pct yield stress at the first quarter cycle, decreases with increasing γ' particle size (Table III). A considerable increase in the degree of hardening with increasing strain amplitude is also observed.

Figure 4 shows the cyclic stress-strain curve of PA material plotted on a log-log scale. The stress and strain values corresponding to maximum hardening state during fatigue are used. This plot exhibits a bilinear behavior with a change of slope at $\Delta\varepsilon_p/2 \approx 0.3$ pct. The values of the cyclic work-hardening exponent n and the constant K in the stress-strain relation $\sigma = K \cdot (\Delta\varepsilon_p/2)^n$ are as follows:

	K (MPa)	n
Region A	2067	0.174
Region B	1427	0.108

Table II. Heat Treatment and Resulting γ' Particle Sizes

Heat Treatment		Average γ' Particle Diameter (nm)	Sample Designation*
Solutionizing Treatment	Aging Treatment		
1313 K-0.5 h oil quenched	1023 K- 8 h	10	UA
	1023 K- 20 h	21	PA
	1023 K-100 h	30	OA

*UA = underaged; PA = peak aged; and OA = overaged.

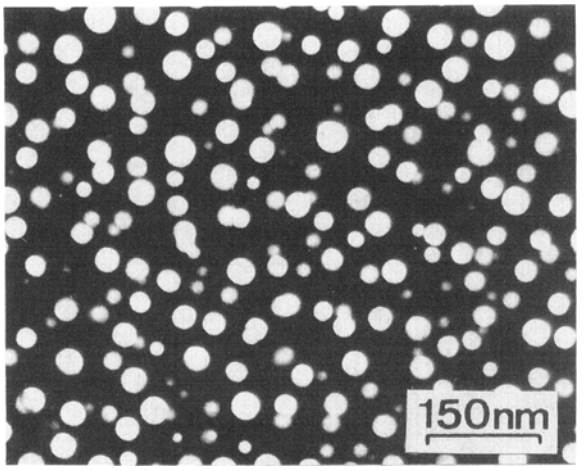

Fig. 1—Dark-field transmission electron micrograph of the PA material showing a typical uniform distribution of γ' particles.

Table III. Cyclic Stress Response Behavior and Fatigue Life of NIMONIC PE16 at Room Temperature*

Material Designation	$\pm\Delta\varepsilon_t/2$ (Pct)	$\pm\Delta\varepsilon_p/2$ (Pct)			$N\sigma_{max}$ (Cycles)	$\Sigma\varepsilon_p^*$ (Pct)	$\sigma_{max}/2$ (MPa)	$\sigma_{max} - \sigma_0$ (MPa)	N_f (Cycles)	N_i
		$N = 1$	$N\sigma_{max}$	$N_f/2$						
UA	0.60	0.28	0.21	0.25	31	26.4	692.2	199.4	7153	6366
	0.72	0.41	0.33	0.39	25	32.8	739.8	247.0	3748	3560
	1.05	0.73	0.61	0.69	17	41.3	837.7	345.0	1431	1372
	2.60	2.25	2.05	2.16	6	49.2	1043.0	550.2	186	174
PA	0.44	0.12	0.09	0.14	21	9.7	669.0	128.0	17,006	—
	0.60	0.29	0.23	0.29	37	34.0	738.3	197.3	5711	5607
	0.70	0.39	0.31	0.38	40	38.4	767.0	226.0	5648	4552
	1.03	0.68	0.57	0.66	14	31.9	844.2	303.2	1884	1700
	2.60	2.13	1.95	2.07	5	39.0	1043.0	502.0	202	195
OA	0.60	0.25	0.18	0.22	129	92.9	705.8	189.2	6763	6632
	0.72	0.38	0.30	0.35	80	96.0	738.0	221.4	5316	4266
	1.11	0.76	0.64	0.69	20	51.2	799.0	282.4	1829	1793
	2.60	2.20	2.04	2.12	5	41.7	983.2	466.6	177	171

*$\Delta\varepsilon_t/2$: total strain amplitude; $\Delta\varepsilon_p/2$: plastic strain amplitude; $N\sigma_{max}$: number of cycles up to σ_{max}; $\Sigma\varepsilon_p^*$: cumulative plastic strain up to σ_{max}, σ_0: 0.02 pct offset tensile yield stress; $\sigma_{max} - \sigma_0$: degree of maximum work hardening; N_f: number of cycles to failure; and N_i: number of cycles for the appearance of asymmetry in hysteresis loops.

The dependence of fatigue life on plastic strain amplitude represented by Coffin-Manson plot for the three initial microstructural states is shown in Figure 5. The data do not reveal any dependence of the fatigue life on the particle size. Since the tests were conducted at constant total strain amplitude and the cyclic plastic strain continually varied with cycles, the value of $\Delta\varepsilon_p/2$ for the Coffin-Manson plot was taken at half-life ($N_f/2$), in conformity with the procedure followed in literature. The X-axis represents the number of reversals to failure, *i.e.*, N_f. This plot exhibits a bilinear behavior with a change of slope occurring at $\Delta\varepsilon_p/2 \approx 0.3$ pct. The slope in the regime of large strain amplitude (region 1) is of the order of -0.54, which lies in the range of the values (-0.5 to -0.6) reported in literature for many other alloy systems.[19] The extrapolation of this plot back to $N_f = 1$ gives the plastic strain amplitude at which fatigue failure occurs after the first quarter cycle. This represents the fracture strain of the material in a monotonic tensile test. The extrapolated value of $\Delta\varepsilon_p/2$ at $N_f = 1$ was 0.52 and matches very well with the value of true fracture strain in tension (0.55). At smaller strain amplitudes, the plot has a higher slope (-0.84). This means that the fatigue life at small strain amplitudes (region 2) is smaller than that expected on the basis of the behavior at large strain amplitudes (region 1).

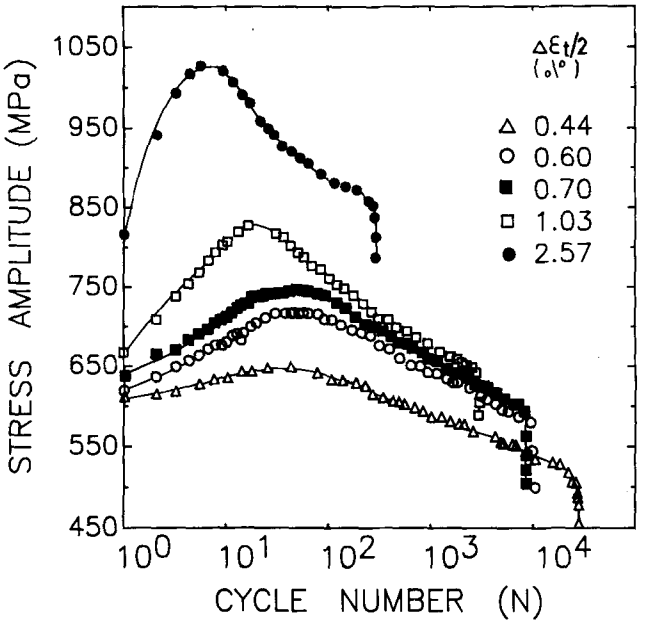

Fig. 2—Cyclic response curves showing the variation of stress amplitude with cycles for the PA material at different total strain amplitudes.

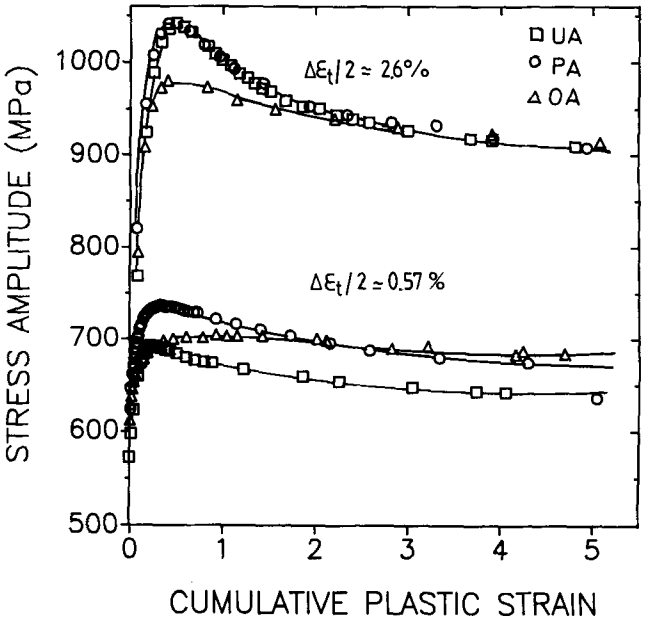

Fig. 3—Cyclic response curves for the UA, PA, and OA materials as a function of cumulative plastic strain tested at $\Delta\varepsilon_t/2 = 0.60$ and 2.60 pct.

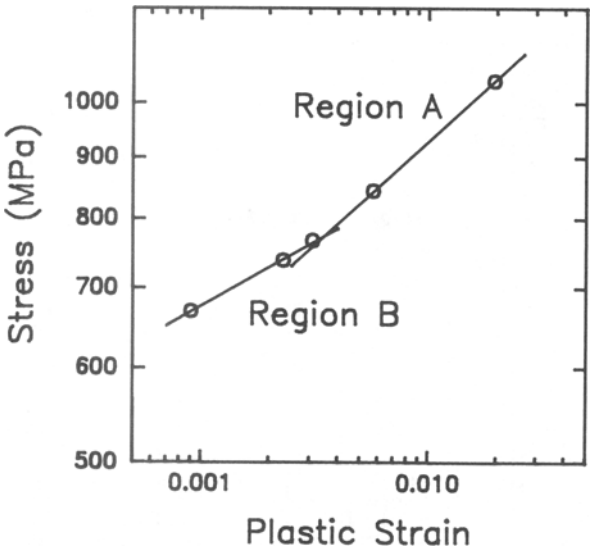

Fig. 4—Cyclic stress-strain curve for the PA material. The stress and strain values are $\Delta\sigma_{max}/2$ and $\Delta\varepsilon_{p,min}/2$, respectively.

C. *Deformation Microstructure*

Figure 6 shows optical micrographs taken from a deformed region of all of the three materials cycled to failure. At low strain amplitudes, the degree of strain homogeneity increases with increasing γ' particle size, as seen by a progressive increase in the density of deformation bands (Figures 6(a) through (c)) and also shown by the increase in the number of grains containing deformation bands. The results of the quantitative measurements ($\Delta\varepsilon_t/2 = 0.60$ pct) concerning this behavior are listed in Table IV. Moreover, it appears that in most of the grains, only one system of parallel {111} planes is activated. Transmission electron microscopic investigation revealed sheared γ' particles and γ' free bands (Figures 7 and 8). In addition, Orowan loops around γ' precipitates were observed in OA material (Figure 8).

Microstructures of samples tested at high strain amplitudes, for both UA and PA materials, revealed multiple slip with a very small interband spacing (Figures 6(d) and (e)). However, the OA material (Figure 6(f)) did not reveal such features even after overetching. The OA specimens showed, in most of the grains, a uniform distribution of etch pits (assumed to be caused by exposure of dislocations on specimen surface), suggesting a homogeneous distribution of dislocations (Figure 6(f)). Slip bands were not observed in this material. Electron microscopic investigations support these observations. A high density of deformation bands is visible in the UA and PA material (Figure 9), whereas in the OA material, a uniform distribution of a high density of dislocations with Orowan loops around γ' particles is noticed (Figure 10).

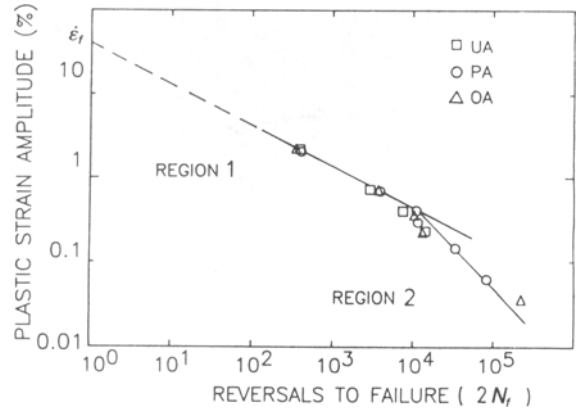

Fig. 5—Coffin-Manson plots of the UA, PA, and OA materials.

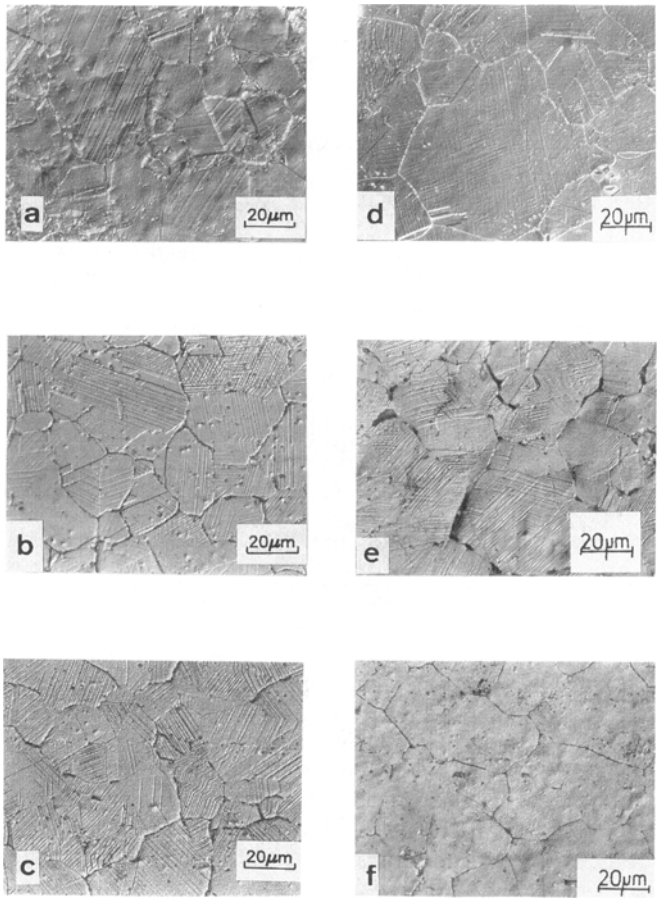

Fig. 6—Optical micrographs showing slip bands in the differently heat-treated specimens tested in LCF at $\Delta\varepsilon_t/2 = 0.60$ pct: (*a*) UA, (*b*) PA, and (*c*) OA and $\Delta\varepsilon_t/2 = 2.60$ pct: (*d*) UA, (*e*) PA, and (*f*) OA.

IV. DISCUSSION

A. *Cyclic Stress Response*

As shown in Figures 2 and 3, all specimens initially hardened to a maximum stress and then softened until failure. This behavior can be explained on the basis of the nature of the internal resistance to deformation of the material. In precipitation-hardened systems, this resistance has two components—one due to dislocation-dislocation interaction (work hardening) and the other due to dislocation-precipitate interaction (precipitation strengthening). On the basis of the known hardening behavior under monotonic loading, the rate of work hardening under LCF loading $(\Delta\sigma/dN)_{\Delta\varepsilon}$ is expected to be

Table IV. Interslip Band Spacing, Deformation Band Width, and Fatigue Life of Different Specimens

Specimen Number	Fracture Life	Interslip Band Spacing (μm)	Percentage of Grains in which Slip is Observed	Mean Deformation Band Width (nm)
UA	9408	4.56 ± 1.75	82	12.5
PA	5711	2.89 ± 0.98	100	25.4
OA	6763	1.91 ± 1.19	100	61.3

large at small plastic strains and to decrease with increasing cumulative strain for a given strain amplitude. The total work hardening should increase to a peak value with increasing number of cycles, whereas the contribution to strength from the shearable precipitates decreases (precipitate softening) with an increase in number of cycles due to a progressive decrease in the effective precipitate cross section. At small cumulative strains, the rate of the precipitate softening is shown to be small but to increase with cumulative strain.[20] The observed initial increase in strength under all experimental conditions (Figures 2 and 3) is therefore essentially due to the work hardening of the matrix caused by a rapid increase in the dislocation density.[20] In the case of shearable precipitates, after some cumulative strain, the rates of work hardening and precipitate softening would become equal, leading to the observed peak in the stress followed by a net softening at larger cumulative strains, since at this later stage precipitate softening dominates over work hardening.[20]

The precipitate softening caused by precipitate shear is also responsible for the deformation to be localized in a few slip planes.[21] The widths and spacings of slip bands given in Table IV allow an estimate of the relative band volumes. The UA material with the smallest band volume shows the highest work hardening (Table III). This is perhaps due to enhanced dislocation-dislocation interaction caused by concentration of dislocations in slip bands.

If the γ' particles were of a size that they cannot be sheared but bypassed by forming dislocation loops around them (Orowan mechanism), these particles would offer increasing resistance to the following dislocations in the same slip plane due to decreased effective interparticle spacing. This would result in forcing out dislocations to adjacent slip planes (for small strain amplitude) or to other

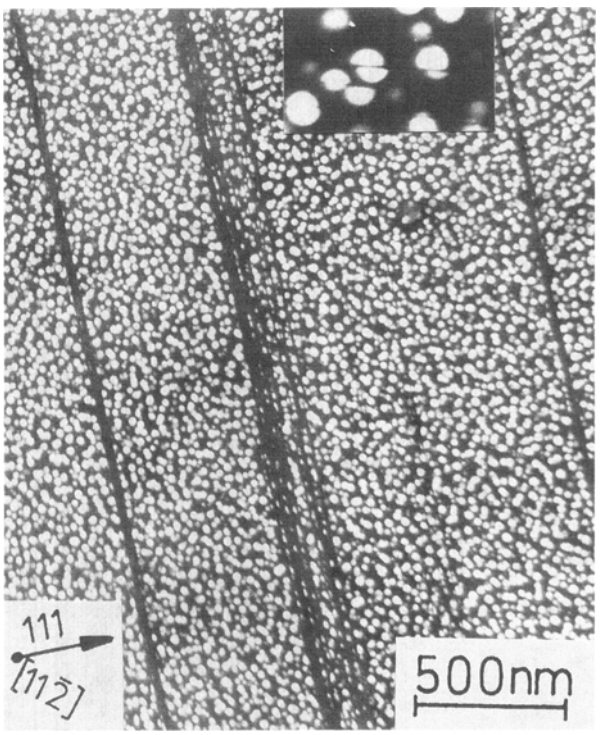

Fig. 7—Dark-field micrograph revealing deformation bands free of γ' particles in the PA material ($\Delta\varepsilon_t/2$ = 0.60 pct). Inset shows magnified view of sheared γ' particles.

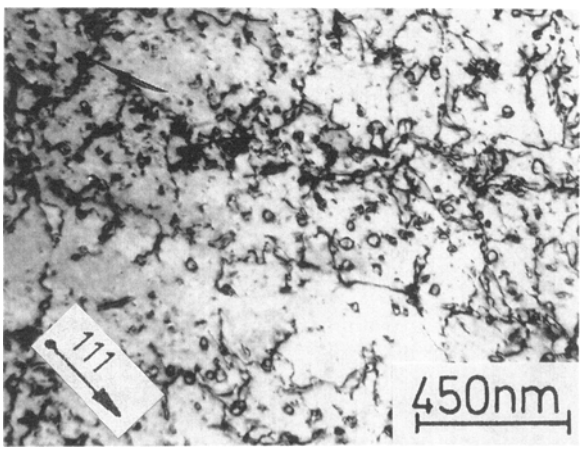

(*a*)

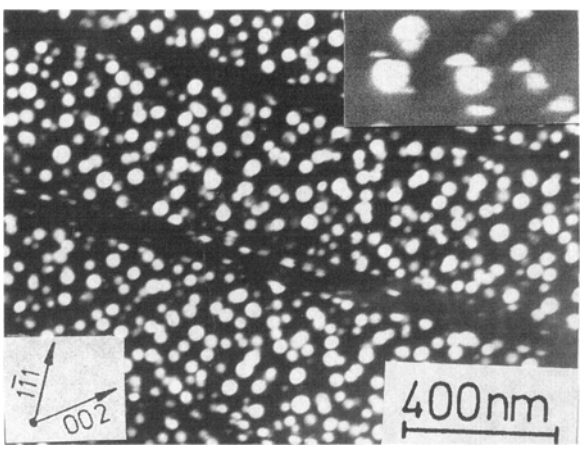

(*b*)

Fig. 8—Deformation microstructure in the OA material tested at $\Delta\varepsilon_t/2$ = 0.60 pct: (*a*) Orowan loops around γ' particles and (*b*) dark-field micrograph revealing γ'-free deformation bands. A magnified view of sheared γ' particles is shown in the inset.

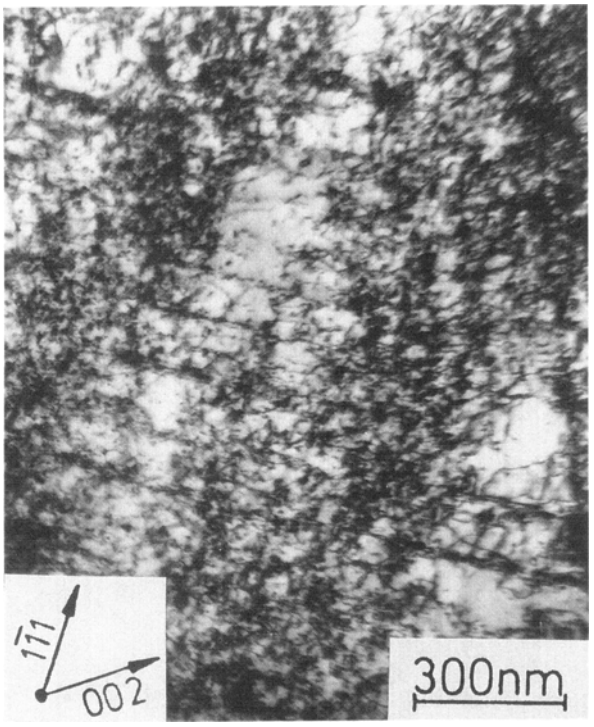

Fig. 9—Distribution of dislocations within closely spaced deformation bands in PA material ($\Delta\varepsilon_t/2$ = 2.6 pct).

slip systems (high strain amplitude). Thus, this type of precipitate-dislocation interaction would result in a relatively homogeneous dislocation distribution, causing a lower peak hardening than that when particle shear is operative. In the present study, the UA and PA materials show only shearing of γ' particles (Figure 7), whereas the OA material shows both γ' shearing and Orowan bypassing (Figure 8). As discussed above, both the degree of hardening and softening are enhanced by γ' shear. In the OA material (d = 30 nm), both of these aspects are expected to be less pronounced, since only some of the γ' precipitates are sheared and the rest are overcome by Orowan mechanism. Thus, the extents of hardening to peak and softening after the peak are less in OA than in UA and PA materials (Table III). This behavior might also be responsible for the shift of maximum peak stress to a higher number of cycles in the OA material (Table III).

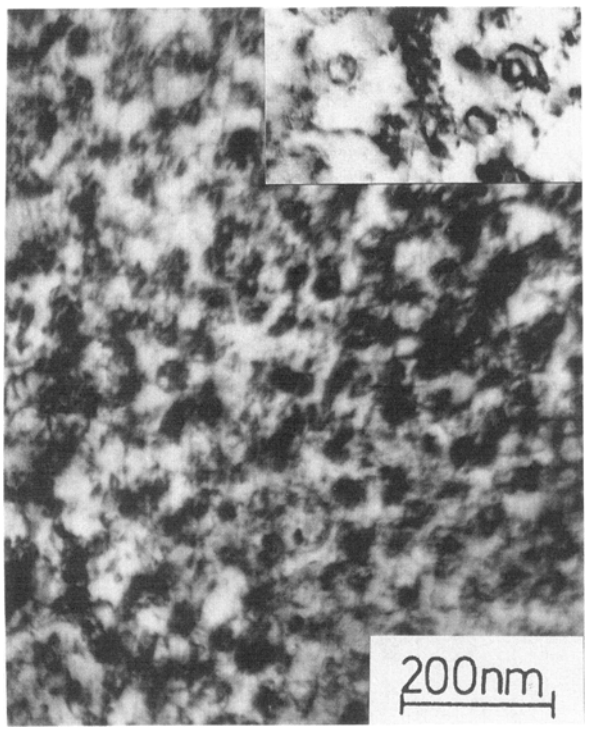

Fig. 10—Uniform distribution of dislocations in deformed OA material ($\Delta\varepsilon_t/2$ = 2.60 pct). A high density of dislocations as well as Orowan loops (see inset) around γ' particles can be seen.

Estimated values of threshold stresses for Orowan and shear mechanisms for the present γ' sizes, following the modified approach suggested in the literature,[22,23] are given in Table V. The threshold stress for an Orowan mechanism is higher than that for shearing. It is clear from the cyclic stress response plot for high strain amplitude (Figure 3) that the Orowan stress for OA material is exceeded by the cyclic stress after a few cycles during deformation. In such a case, as observed, both shearing of the γ' particles and Orowan looping would take place. In the case of the UA and PA material, the respective threshold stresses for the Orowan mechanism are quite high and are never reached during deformation, so that the deformation takes place essentially through particle shear.

Our observation for the occurrence of the maximum stress over a narrow range of cycles at small strain amplitudes ($\Delta\varepsilon_p/2 < 0.3$ pct) for shearable precipitates (UA and PA materials) is consistent with that reported in the literature on other nickel-base alloy systems.[11,13] Lerch *et al.*[10] have shown that the slip band spacing decreases with increasing $\Delta\varepsilon_t/2$. Stolz and Pineau[13] observed that the number of slip bands increased linearly with plastic strain amplitude in WASPALOY. They suggested that if the kinetics of hardening and softening within each slip band are independent of strain amplitude, the stress maximum should be achieved within a constant number of cycles. This behavior is typical of low strain amplitudes where only a single slip system is activated.

At higher strain amplitudes, the maximum stress is achieved in a small number of cycles for all γ' particle sizes. This might be a result of the rapid increase in the density of slip bands and the activation of various slip systems, which increase the dislocation density to the saturation value within the first few cycles.

It is interesting to note that for large strain amplitudes, the cyclic stress response plots of UA and PA material

Table V. Estimated Values of Orowan and Shear Threshold Stresses for Different γ' Particle Sizes at Room Temperature

Average Particle Diameter (nm)	Orowan Stress, σ_{Or} (MPa)	Shear Stress, σ_s (MPa)
10	1692	461
21	1053	574
30	799	660

merge into a single curve (neglecting very small differences in the plastic strain amplitude between these samples). In NIMONIC 80A, Lerch and Gerold[12] observed that there is only one stress associated with particular slip band spacing in the high strain amplitude regime irrespective of the precipitate size. They suggest that the number of slip bands is directly responsible for hardening and not the precipitate size. Our TEM investigation reveals that the slip band spacing at large strain amplitudes is very small and the interband regions also contain a high density of dislocations (Figure 9). Dislocation-dislocation interaction is justifiably more dominant over dislocation-precipitate interaction in this regime of high strain for UA and PA materials. The dislocation density is too high to carry out any quantitative measurements, and it is reasonable to assume that they are close to a saturation value. Hence, in light of Lerch and Gerold's suggestion, it is not surprising that both response curves merge together. In the case of the OA material, dislocations are uniformly distributed with loops around the γ' particles, and no well-defined bands were observed (Figure 10). In the case of the OA material, the nature of work hardening is influenced by the Orowan mechanism. This work-hardening behavior is different from that in the UA and PA materials and is reflected in the observed difference in their stress responses.

B. *Cyclic Stress-Strain Behavior*

The cyclic stress-strain plot (Figure 4) shows a change of slope at about 0.3 pct plastic strain amplitude. Similar behavior has been observed in NIMONIC 80A[12] and WASPALOY,[24] and it has been related to the change in the deformation mechanism from dislocation glide to microtwinning at low strain amplitudes and grain rotation at high plastic strain amplitudes. In the present study, no microtwinning is observed. However, there is a change in the number of slip systems operating between small and large strain amplitudes. Generally, at $\Delta\varepsilon_p/2 < 0.3$ pct, a single slip system is activated within most of the grains (Figures 6(a) through (c)). At higher strain amplitudes, multiple slip takes place within all grains. The interslip band spacing reduces drastically (Figures 6(d) through (f)). Transmission electron microscopic examination revealed the spacing to be of the order of a few nanometers. A much stronger dislocation-dislocation interaction is expected and would lead to, as observed in Figure 4, a higher work hardening than in the case of single slip. A similar change in the slip characteristic (single and multiple) between low and high strain amplitudes in this alloy has been observed in an earlier investigation.[15]

C. *Fatigue Life*

The Coffin-Manson plot also shows a change of slope at 0.3 pct (Figure 5). The slope of the plot in the region of large strain amplitude (region 1) is of the order of 0.54, which is typical of many metals and alloys. However, at small strain amplitudes, the slope of the plot (region 2 in Figure 5) has a higher value of 0.84. It is obvious that for the same strain amplitude, the fatigue life in region 2 is less than that expected from an extrapolation of region 1. This behavior can be understood as follows: total life to failure $N_f = N_i + N_p$ (i and p = crack initiation and propagation, respectively). Hornbogen and Zum Gahr[25] suggest that crack initiation starts only after a particular glide step height has been reached in the slip plane. The number of cycles required to achieve this step height decreases with increasing degree of inhomogeneity in deformation for the same strain. This means that for the same strain amplitude, the material in which dislocations are inhomogeneously distributed will have a smaller N_i compared to one in which dislocations are uniformly distributed. The value of N_p in the present study is negligibly small (about 10 pct of N_f; see Table III), so that $N_f \approx N_i$. This explains the shorter life at small $\Delta\varepsilon_t/2$ as compared to that expected on the basis of an extrapolation of the data at large $\Delta\varepsilon_t/2$ to smaller values.

V. CONCLUSIONS

1. The nature of the cyclic stress response curve is determined by the operating dislocation-precipitate interaction mechanism. When precipitate shearing is the dominant mechanism (UA and PA states), the initial hardening is followed by a period of softening. For the OA state, where both Orowan looping and precipitate shearing are operating, the extents of hardening and softening are relatively small.
2. At low strain amplitudes ($\Delta\varepsilon_p/2 \leq 0.70$ pct), the maximum response stress in UA and PA materials is attained within a narrow range of cycles. However, at higher strain amplitudes, the number of cycles to achieve maximum stress shifts to lower values. On the other hand, for OA state, the number of cycles for maximum stress continuously decreases with increase in strain amplitude.
3. The cyclic stress-strain curve and Coffin-Manson plot show a bilinear behavior with a change of slope at a plastic strain amplitude $\Delta\varepsilon_p/2$ of 0.3 pct. This change in the behavior is associated with the change in deformation from single slip to multiple slip.

ACKNOWLEDGMENTS

The authors would like to thank Mrs. S. Weber, Miss D. Köpnick, Mr. G. Pruskil, and Mr. J. Anderl for their technical assistance. The authors are grateful to Professors D. Aurich, H. Wever, and H. Wollenberger for their permanent support. The work was supported by the Stiftung "Volkswagenwerk."

REFERENCES

1. H. Mughrabi: *Proc. Conf. on 50th Anniversary of the Concept of Dislocations in Crystals*, Institute of Metals, London, 1984, p. 244.
2. C. Laird, P. Charsley, and H. Mughrabi: *Mater. Sci. Eng.*, 1986, vol. 81, pp. 433-50.
3. D. Steiner and V. Gerold: *Mater. Sci. Eng.*, 1986, vol. 84, pp. 77-88.
4. C. Calabrese and C. Laird: *Mater. Sci. Eng.*, 1974, vol. 13, p. 141.
5. J.K. Lee and C. Laird: *Mater. Sci. Eng.*, 1982, vol. 54, pp. 53-64.
6. S.D. Antolovich: *La Fatigue des Matériaux des Structures*,

C. Bathias and J.P. Bailon, eds., Maloine, Paris, 1980, pp. 465-596.
7. S.D. Antolovich, S. Liu, and R. Baur: *Metall. Trans. A*, 1981, vol. 12A, pp. 473-81.
8. L.G. Fritzmeier and J.K. Tien: *Acta Metall.*, 1988, vol. 36, pp. 275-82.
9. L.G. Fritzmeier and J.K. Tien: *Acta Metall.*, 1988, vol. 36, pp. 283-90.
10. B. Lerch, N. Jayaraman, and S.D. Antolovich: *Mater. Sci. Eng.*, 1984, vol. 66, pp. 151-66.
11. B. Lerch and V. Gerold: *Acta Metall.*, 1985, vol. 33, pp. 1709-16.
12. B. Lerch and V. Gerold: *Metall. Trans. A*, 1987, vol. 18, pp. 2135-41.
13. R.E. Stolz and A.G. Pineau: *Mater. Sci. Eng.*, 1978, vol. 34, pp. 275-84.
14. D.L. Anton and M.E. Fine: *Metall. Trans. A*, 1982, vol. 13, pp. 1187-98.
15. C.H.D. Arbuthnot: *Fracture and the Role of Microstructure*, Chameleon Press Ltd., London, United Kingdom, 1982, pp. 407-13.
16. H.P. Degischer, W. Hein, H. Strecker, W. Wagner, and R.P. Wahi: *Z. Metallkd.*, 1987, vol. 78, pp. 237-49.
17. R.P. Wahi, V.V. Kutumbarao, H.M. Yun, and W. Chen: in *Low Cycle Fatigue and Elasto-Plastic Behavior of Metals*, Elsevier Applied Science, London, 1987, pp. 290-95.
18. V. Singh, W. Chen, H.M. Yun, and R.P. Wahi: *Scripta Metall.*, 1988, vol. 22, pp. 77-79.
19. S.S. Manson and G. Halford: in *Thermal and High Strain Fatigue*, The Metals and Metallurgy Trust, London, 1967, p. 154.
20. R.P. Wahi, W. Chen, V. Singh, and V.V. Kutumbarao: *Festigkeit und Verformung bei hoher Temperatur*, K. Schneider, ed., DGM-Informationsgesellschaft mbH, Oberursel, Federal Republic of Germany, 1989, p. 219.
21. M. Sundararaman, V. Singh, W. Chen, and R.P. Wahi: *Acta Metall. Mater.*, 1989, vol. 38, pp. 1813-22.
22. W. Hüttner and B. Reppich: *Z. Metallkd.*, 1978, vol. 69, p. 628.
23. E. Nembach and G. Neite: *Prog. Mater. Sci.*, 1985, vol. 29, pp. 177-319.
24. M. Clavel, A. Pineau, G. Chalant, and L. Remy: in *Fatigue Threshold*, Proc. 1st Int. Conf., J. Bäcklund, A. Blom and C.J. Beevers, eds., Stockholm, EMAS, Warley, United Kingdom, 1981, pp. 191-203.
25. E. Hornbogen and K.H. Zum Gahr: *Scripta Metall.*, 1978, vol. 12, pp. 147-50.